DISCRETE AND CONTINUOUS
DYNAMICAL SYSTEMS
Volume **32**, Number **8**, August **2012**

doi:10.3934/dcds.2012.32.2951

pp. **2951–2970**

WAVES IN RANDOM NEURAL MEDIA

Stephen Coombes and Helmut Schmidt

School of Mathematical Sciences
University of Nottingham
Nottingham, NG7 2RD, UK

Carlo R. Laing

Institute of Information and Mathematical Sciences
Massey University
Private Bag 102-904, North Shore Mail Centre, Auckland, New Zealand

Nils Svanstedt

Mathematical Sciences
Chalmers University of Technology and University of Gothenburg
S-412 96 Göteborg, Sweden

John A. Wyller

Department of Mathematical Sciences and Technology
Norwegian University of Life Sciences
P. O. Box 5003, NO-1432 Ås, Norway

Abstract. Translationally invariant integro-differential equations are a common choice of model in neuroscience for describing the coarse-grained dynamics of cortical tissue. Here we analyse the propagation of travelling wavefronts in models of neural media that incorporate some form of modulation or randomness such that translational invariance is broken. We begin with a study of neural architectures in which there is a periodic modulation of the neuronal connections. Recent techniques from two-scale convergence analysis are used to construct a homogenized model in the limit that the spatial modulation is rapid compared with the scale of the long range connections. For the special case that the neuronal firing rate is a Heaviside we calculate the speed of a travelling homogenized front exactly and find how the wave speed changes as a function of the amplitude of the modulation. For this special case we further show how to obtain more accurate results about wave speed and the conditions for propagation failure by using an interface dynamics approach that circumvents the requirement of fast modulation. Next we turn our attention to forms of disorder that arise via the variation of firing rate properties across the tissue. To model this we draw parameters of the firing rate function from a distribution with prescribed spatial correlations and analyse the corresponding fluctuations in the wave speed. Finally we consider generalisations of the model to incorporate adaptation and stochastic forcing and show how recent numerical techniques developed for stochastic partial differential equations can be used to determine the wave speed by minimising the L^2 norm of a travelling disordered activity profile against a fixed test function.

2000 *Mathematics Subject Classification.* Primary: 45J05; Secondary: 92C20.

Key words and phrases. Integro-differential equations, neural field models, homogenization, random media.

1. **Introduction.** There is now a long history of the use of integro-differential equations in modelling the coarse-grained activity of neural tissue, as reviewed in [1]. Many current models are variations on the standard Wilson-Cowan [2, 3] or Amari model [4, 5] and take the form

$$u_t(x,t) = -u(x,t) + \int_{-\infty}^{\infty} \mathrm{d}y\, w(x,y) f(u(y,t)). \tag{1}$$

Here, $u(x,t)$ is interpreted as a neural field representing the local activity of a population of neurons at position $x \in \mathbb{R}$ (and generalisations of the model to higher dimensions is straight-forward). The second term on the right represents the synaptic input, with f interpreted as the firing rate function. A common choice for this is a smooth sigmoidal function of the form

$$f(u) = \frac{1}{1+\mathrm{e}^{-\beta(u-h)}}, \tag{2}$$

where $\beta > 0$ sets the gain and h the threshold. The strength of anatomical connections between neurons at positions x and y is denoted $w(x,y)$. These are often assumed to be homogeneous so that $w(x,y) = w(|x-y|)$ and the system becomes translationally invariant. From a mathematical perspective this is particularly useful for analysing travelling waves, which can be constructed as stationary profiles in a co-moving frame. Indeed there is considerable interest in waves in neural tissue since they underlie both natural and pathological neurobiological phenomena. An example of the former is spreading excitation associated with sensory processing [6], while waves in epilepsy are a classic example of the latter [7]. In the special case that f is a Heaviside function then the dependence of wave velocity (and stability) on the shape of the homogeneous connectivity can be analysed exactly (reviewed in [1]). However, analogous results for heterogeneous systems are much harder to come by and even the existence and uniqueness of solutions to (1) has only been treated recently [8]. For the particular case that the connectivity has the form $w(x,y) = w(|x-y|)[1+J(y/\gamma)]$ with J some periodic function, which models the *patchiness* of connections seen in cortex, Bressloff [9] has shown how averaging methods can be tailored to treat non-local neural models like (1) and allow for the analysis of waves in the limit $\gamma \to 0$. Moreover, he was able to obtain explicit results for wave speeds and the conditions for propagation failure in the case of a Heaviside firing rate. For this special case Schmidt *et al.* [10] and later Coombes and Laing [11] were able to obtain improved results valid away from the limit $\gamma = 0$. The analysis of waves in truly inhomogeneous (as opposed to periodically modulated) neural media is a much harder problem, though one that will have a huge bearing on our understanding of how waves propagate throughout the brain. To date it appears that the only work in this area is that of Brackley and Turner, who make extensive (though not exclusive) use of simulations to study the role of inhomogeneities in connectivity [12] and fluctuations in the firing rate function [13] on wave propagation. These are precisely the topics we address in this paper, as well as laying a firmer foundation for the analysis of periodically modulated neural fields.

In section 2 we introduce a rigorous equation for a homogenized model of periodically modulated neural media, making use of recent ideas from two-scale convergence analysis. For a Heaviside firing rate we show how to calculate the speed of a travelling front in this system. Next we show in section 3 that for this special case one

can side-step the use of homogenization theory and develop an alternative perturbative analysis which tracks the position of the wave interface with a greater degree of accuracy. Numerical simulations are presented to highlight both the regime of validity of the homogenization calculations and the improved performance of the interface approach where they break down. We break translation invariance again in section 4, though this time by treating the firing threshold as a random variable. A theory that relates fluctuations in the threshold to fluctuations in wave speed is developed and shown to be in excellent agreement with numerical simulations. In this section we also treat the case of noise driven neural fields (generalised now to include adaptation) and develop a numerical technique for the determination of wave speed based on recent *freezing* techniques developed for the study of stochastic partial differential equations. Finally in section 5 we discuss further challenges for the study of waves in random neural media.

2. **Homogenization for periodically modulated connectivities.** To incorporate the known microstructure of visual cortex within a large-scale modelling framework Bressloff has proposed the use of periodically modulated connectivity kernels [9]. Moreover, if the variation on the micro scale is rapid compared with that on the large scale then the use of homogenization techniques is appropriate. Homogenization is traditionally associated with the study of partial differential equations with rapidly oscillating coefficients, as done by Keener for models of cardiac dynamics with rapidly varying spatial structure [14]. This technique, whereby an equation with a highly oscillatory coefficient is replaced by one with a homogeneous (uniform) coefficient, has been extended to non-local neural field models by Bressloff [9], who used formal perturbation techniques to derive a hierarchy of expressions for determining wave-speeds. However, the actual homogenized model (to which the perturbation theory would apply) was not explicitly discussed. In this section we summarise some of the key ideas and steps from two-scale convergence that allow one to construct the homogenized version of (1). As well as allowing for connectivities that are periodically modulated, as treated in [9, 10, 11], we shall also allow for ones that have a periodic modulation of their spatial scale. To be more precise we consider kernels of the form

$$w(x,y)=\frac{1}{\sigma_1(y/\gamma)}\phi\left(\frac{|x-y|}{\sigma_2(y/\gamma)}\right). \tag{3}$$

The functions $\sigma_{1,2}$ are assumed to be strictly positive and smooth with period one, i.e. $\sigma_{1,2}(y)=\sigma_{1,2}(y+1)$ for all y. The function ϕ is a scaling function which by assumption is integrable. The parameter $0<\gamma\ll 1$ defines the period of the microvariation. σ_1 can be used to model a medium with a periodically modulated connection strength, while σ_2 can allow for modulation of some long range spatial scale. For simplicity we shall set $\sigma_1=\sigma_2=\sigma$ from now on (though stress that a full analysis can be developed which treats these separately). The problem now consists of deriving the limit equation as $\gamma\to 0$ i.e. of homogenizing the model defined by (1)–(3). It turns out that we can carry out this derivation in a rigorous and efficient way by means of the two-scale convergence technique originally developed by Nguetseng [15]. The homogenized model is given as

$$u_t(x,y,t)=-u(x,y,t)+\int_{-\infty}^{\infty}\mathrm{d}x'\int_0^1\mathrm{d}y' w^*(x-x',y-y')f(u(x',y',t)), \tag{4}$$

where

$$w^*(x,y) = \frac{1}{\sigma(y)}\phi\left(\frac{|x|}{\sigma(y)}\right), \tag{5}$$

and is independent of γ. Here y represents some fast variable that would typically occur in a solution expansion of the form $u(x,t) = u_0(x,t) + \gamma u_1(x,y,t) + \gamma^2 u_2(x,y,t) + \mathcal{O}(\gamma^3)$ with $y = x/\gamma$. In Appendix A we sketch the main ideas in the derivation of (4). A notable feature of the homogenized model is that the effect of the oscillatory synaptic footprint is stored in the spatial two-scale limit of the connectivity kernel w^*.

In the next several sections of this paper we shall work with the concrete choice $w(x,y) = w^*(x-y, y/\gamma)$ where

$$\phi(x) = \frac{1}{2}\mathrm{e}^{-|x|}, \qquad \sigma(y) = 1 + \alpha\sin(2\pi y). \tag{6}$$

For $\alpha = 0$ we recover a model that is translationally invariant, and as γ is decreased toward zero we expect the homogenized model to become increasingly accurate. In Fig. 1 we show a sequence of simulation results of the full (unhomogenized model) for various values of α. This nicely highlights the ability of the model to support travelling waves and the fact that they transition from a travelling to a pulsating front (in which the wake has periodic spatial structure) with increasing α. Next we show how the homogenized model can be explicitly analysed for the special case that the firing rate is a Heaviside function and obtain a formula for the homogenized front speed as a function of α.

2.1. **Travelling front.** Here we seek travelling wave solutions of the homogenized model (4). Introducing a co-moving frame $\xi = x - ct$, with $c > 0$, we see that solutions of the form $u(x,y,t) = q(x-ct)$ (independent of y) satisfy

$$-c\frac{\mathrm{d}q}{\mathrm{d}\xi} = -q + \int_{-\infty}^{\infty}\mathrm{d}x'\int_0^1 \mathrm{d}y' w^*(x',y')f(q(\xi - x')), \tag{7}$$

where we have used the fact that the kernel is periodic in y with $w^*(x,y) = w^*(x,y+1)$. For the case that $f(u) = H(u-h)$, where H is a Heaviside function, we see that travelling front solutions with $q > h$ for $\xi < 0$ and $q < h$ for $\xi > 0$ are given by

$$-c\frac{\mathrm{d}q}{\mathrm{d}\xi} = -q + \int_{\xi}^{\infty}\mathrm{d}x' W(x'), \quad W(x) = \int_0^1 \mathrm{d}y w^*(x,y). \tag{8}$$

This can be integrated to give

$$q(\xi) = \frac{1}{c}\int_0^{\infty}\mathrm{d}\xi' e^{-\xi'/c}G(\xi'+\xi), \qquad G(\xi) = \int_{\xi}^{\infty}\mathrm{d}x' W(x'). \tag{9}$$

The wave speed is determined from the condition $q(0) = h$. For $\xi > 0$, and using (6), we find

$$G(\xi) = \frac{1}{2}\int_0^1 \mathrm{d}y \mathrm{e}^{-\xi/\sigma(y)}. \tag{10}$$

Hence, from (9) with $\xi = 0$, the speed is determined by

$$h = \frac{1}{2} - \frac{1}{2}\int_0^1 \mathrm{d}y \frac{c}{\sigma(y)+c}, \qquad \alpha < 1. \tag{11}$$

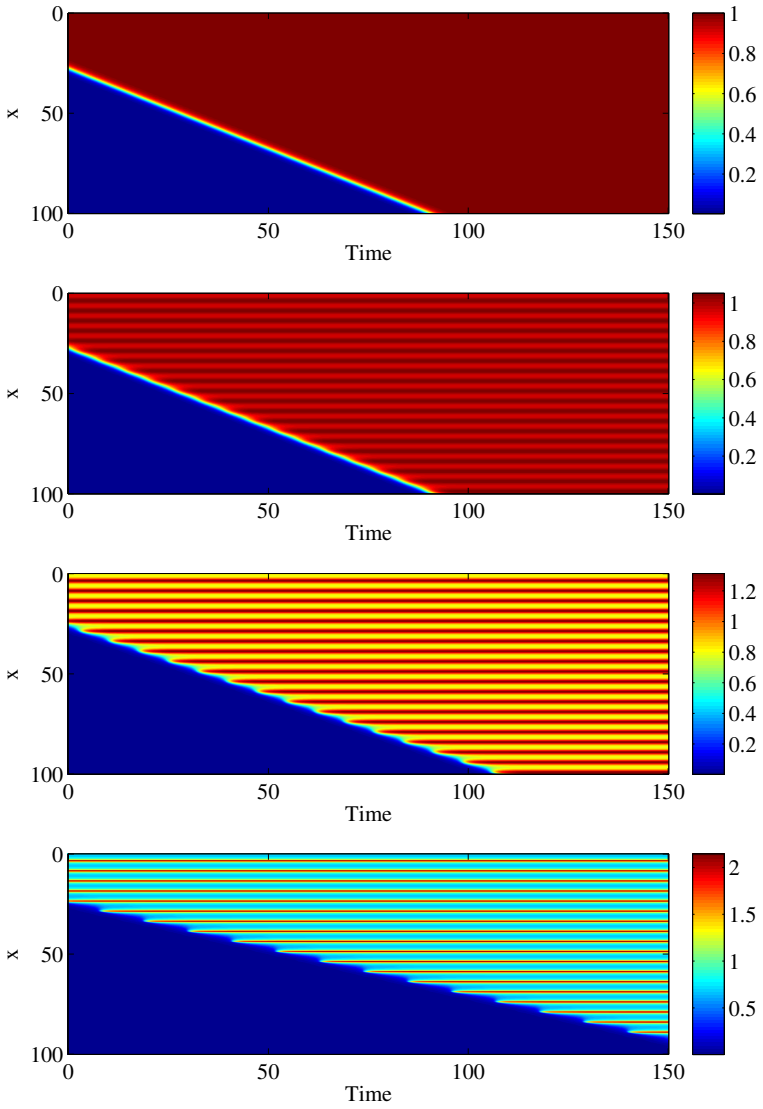

FIGURE 1. Simulations of (1)-(6) for (top to bottom) $\alpha = 0$, 0.1, 0.5 and 0.9. $u(x,t)$ is shown color-coded. Other parameters are $h = 0.3$, $\beta = 20$ and $\gamma = 5$.

Using a half angle substitution we may solve this to give

$$c = 2\kappa \left\{ \frac{-2\kappa + \sqrt{1 + \alpha^2(4\kappa^2 - 1)}}{4\kappa^2 - 1} \right\}, \tag{12}$$

where $\kappa = h - 1/2$. A plot of $c = c(\alpha)$ is shown in Fig. 2. Corresponding wave profiles from (9) are shown in Fig. 3. In the limit $\alpha \to 0$ we recover the result for

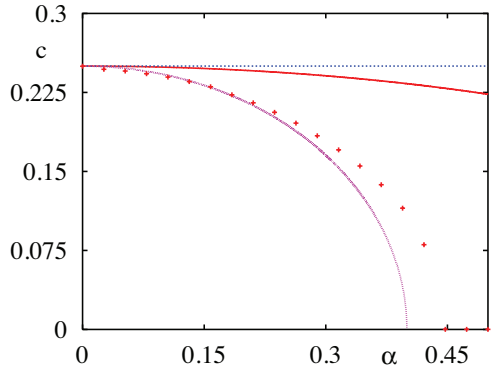

FIGURE 2. A plot of $c = c(\alpha)$ for the case of a travelling front calculated for a Heaviside firing rate with threshold $h = 0.4$ in the homogenized model (solid line, red). Also shown are simulation results for $\gamma = 2\pi$ (crosses, red) as well as a theoretical curve (dotted line, magenta) obtained from an interface dynamics calculation.

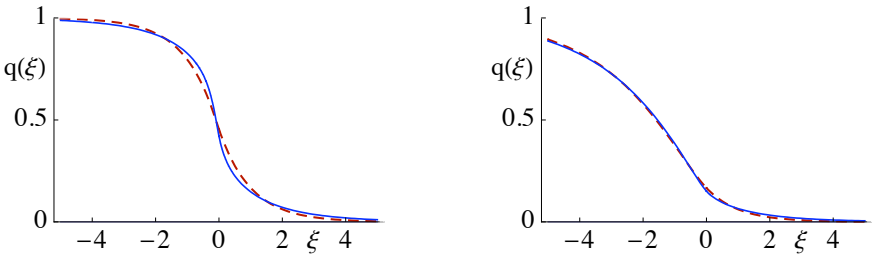

FIGURE 3. Wave fronts (solid lines) in the co-moving frame for $c = 0.1$ (left) and $c = 2$ (right), with $\alpha = 0.9$. Dashed curves are the fronts in the homogeneous model for the same wave speeds.

the homogeneous model (no modulation):

$$c = \frac{1-2h}{2h}. \tag{13}$$

As expected there is good agreement between the analysis of the homogenized model and simulations of the full model only for small α. Also shown in this figure is another theoretical curve, with better agreement over a larger range of α. The derivation of this curve side-steps the need for homogenization theory, though is only valid in the special case that $f(u) = H(u-h)$. We explain this result next.

3. **Beyond homogenization.** Following ideas recently developed in [11] for the study of periodically modulated weight kernels of the form $w(x,y) = \phi(|x-y|)\sigma(y/\gamma)$, we seek to describe the properties of fronts in terms of the behavior at the interface which separates high activity from low. If the front is not pulsating (which is the case in the absence of period modulation) then in a travelling wave frame (of the same speed as the wave) the rising edge of the front may be identified with a single (travelling wave) co-ordinate. For a pulsating front this point is no longer stationary

in time and instead oscillates. We now show how to derive the dynamics for this *interface* between high and low activity states.

In a co-moving frame the model (1) takes the form $u = u(\xi, t)$ where $\xi = x - c_0 t$ for some fixed c_0 and

$$-c_0 u_\xi + u_t = -u + \psi, \tag{14}$$

where

$$\psi(\xi, t) = \int_{-\infty}^{\infty} \mathrm{d}y w(\xi + c_0 t, y) f(u(y - c_0 t, t)). \tag{15}$$

We define a moving interface (level set) according to

$$u(\xi_0(t), t) = h, \tag{16}$$

for some constant h. Here we are assuming that there is only one point on the interface (though in principle we could consider a set of points). Differentiation of (16) gives an exact expression for the velocity of the interface in the form

$$\dot{\xi}_0 = -\frac{u_t}{u_\xi}\bigg|_{\xi=\xi_0(t)}. \tag{17}$$

Focusing now on the case of a Heaviside firing rate with $f(u) = H(u - h)$ means that for a pulsating front solution with $u > h$ for $\xi < \xi_0$ (15) takes the simple form

$$\psi(\xi, t) = \int_{-\infty}^{\xi_0 + c_0 t} \mathrm{d}y w(\xi + c_0 t, y). \tag{18}$$

3.1. **Perturbation analysis.** We now consider the case of small α and expand $w(x, y)$ using (6), as

$$w(x, y) \simeq \phi(x - y)[1 + \alpha(|x - y| - 1)\sin(2\pi y/\gamma)]. \tag{19}$$

For $\alpha = 0$ there is a travelling front $q(\xi)$ given by the solution of

$$-c_0 \frac{\mathrm{d}q}{\mathrm{d}\xi} = -q + \psi, \qquad \psi(\xi) = \int_{\xi}^{\infty} \mathrm{d}y \phi(y), \tag{20}$$

where the speed c_0 is determined by $q(0) = h$. For small α we assume that the slope of the travelling front varies sufficiently slowly so that we may make the convenient approximation $u_\xi|_{\xi=\xi_0(t)} = q_\xi|_{\xi=0}$. In this case we have, using equations (14) and (20), that

$$u_t|_{\xi=\xi_0(t)} = \int_{-\infty}^{\xi_0 + c_0 t} \mathrm{d}y w(\xi_0 + c_0 t, y) - \int_0^{\infty} \mathrm{d}y \phi(y), \tag{21}$$

$$u_\xi|_{\xi=\xi_0(t)} = \frac{1}{c_0}\left(h - \int_0^{\infty} \mathrm{d}y \phi(y)\right). \tag{22}$$

Substitution of equations (21) and (22) into equation (17) gives

$$\dot{\xi}_0 = \alpha c_0 \frac{\int_0^{\infty} \mathrm{d}y \phi(y)(|y| - 1)\sin(2\pi(\xi_0 + c_0 t - y)/\gamma)}{h - \int_0^{\infty} \mathrm{d}y \phi(y)}. \tag{23}$$

Performing the integrals in (23) we find that the time-dependent speed of the front is given by $c_0(1 + \alpha a(\xi_0, t))$ where $c_0 = (1 - 2h)/(2h)$ and

$$a(\xi_0, t) = A \sin\left[\frac{2\pi}{\gamma}(\xi_0 + c_0 t) - \phi\right], \tag{24}$$

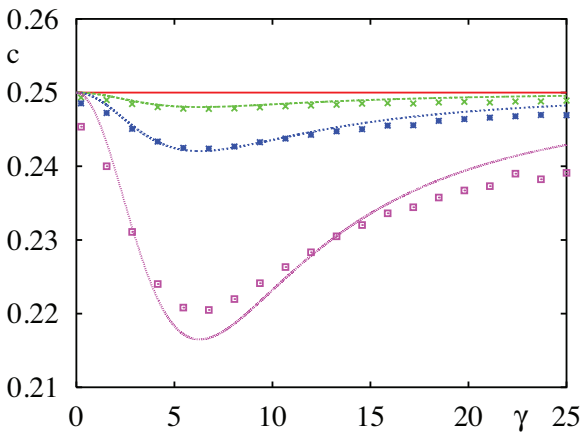

FIGURE 4. Wave speed as determined from an interface dynamics analysis when $h = 0.4$. The horizontal line (red) shows the speed in the unmodulated case where $\alpha = 0$. The three sets of data points (measured from simulations) and the solid lines (calculated from (28)) correspond to $\alpha = 0.05$, $\alpha = 0.1$ and $\alpha = 0.2$ (upper to lower, respectively).

with

$$A = \frac{1}{1-2h}\frac{2\pi/\gamma}{1+(2\pi/\gamma)^2}, \quad \tan\phi = \frac{\pi}{\gamma}\frac{(2\pi/\gamma)^2-1}{(2\pi/\gamma)^2}. \tag{25}$$

Pulsating fronts are T-periodic solutions of the non-autonomous ordinary differential equation (23) with $\xi_0(t) = \xi_0(t+T)$. Introducing $x_0 = \xi_0 + c_0 t$ with $x_0 \in [0, \gamma]$ we may solve for the trajectory using

$$\int_0^{x_0} \frac{\mathrm{d}x}{1+\alpha A \sin(2\pi x/\gamma - \phi)} = c_0 t. \tag{26}$$

Using a half angle substitution we may evaluate this to give

$$c_0 t = \frac{\gamma}{\pi}\frac{1}{a}\tan^{-1}\frac{z}{a}\Big|_{z_0(0)+\alpha A}^{z_0(t)+\alpha A}, \qquad a^2 = 1-\alpha^2 A^2, \tag{27}$$

where $z_0(t) = \tan[(2\pi x_0(t)/\gamma - \phi)/2]$ and $x_0(0) = 0$. A periodic pulsating front with speed $c = \gamma/T$ can be found by demanding that $\gamma = x_0(T)$. Substitution of this condition into (27) shows that the speed of the pulsating front is given by

$$c = c_0\sqrt{1-\alpha^2 A^2}. \tag{28}$$

Hence, a propagating wave is only supported if $|\alpha| < 1/|A|$. We note that the wave speed has a minimum when $\gamma = 2\pi$.

A plot of the wave speed as a function of the spatial scale γ is shown in Fig. 4. We see good agreement between the theoretical prediction from the interface dynamics approach and direct numerical simulations. Indeed this is much better than would be predicted from the analysis of the homogenized model, since in that case the speed is independent of γ. Although our analysis in this case is restricted to small α we have not had to make any assumptions about the scale of periodic modulation as determined by the parameter γ. In contrast a homogenization analysis would

require both small α *and* a periodic modulation that occurs on a smaller length-scale than the correlation length of $\phi(x)$ (which is set to unity here). Returning to Fig. 2, the dotted magenta line shown there, which agrees well with simulation results, is calculated using (28).

4. **Disordered neural fields.** Until now we have only discussed systems with periodic modulation as opposed to true disorder. A general theory for the analysis of arbitrary inhomogeneous connectivities is clearly a challenge and to date has mostly been investigated using numerical simulations. However, it is worth pointing out that time-independent solutions of (1) with $f(u) = H(u-h)$ may allow for further investigation since they are simply given by

$$U(x) = \int_\Omega \mathrm{d}y w(x,y), \qquad \Omega = \{x \mid U(x) > h\}. \tag{29}$$

For example, a pinned front defined by $U(x) > h$ for $x < \eta$ and $U(x) \leq h$ otherwise, is given by

$$U(x) = \int_{-\infty}^{\eta} \mathrm{d}y w(x,y), \tag{30}$$

with η determined by the condition $U(\eta) = h$. Moreover (following arguments in [11]), $U(x)$ is stable if $\lambda < 0$ where

$$\lambda = -1 + \frac{w(\eta,\eta)}{|U'(\eta)|}. \tag{31}$$

Interestingly, for Heaviside firing rates, Brackley and Turner [12] have shown numerically that neural field models with random inhomogeneous connectivities can support coherent fluctuating time-dependent states when the inhomogeneity has an appropriate power-law scaling. Another natural way to generate fluctuations in neural field dynamics is to allow parameters of the model to fluctuate in both space and time, allow parameter heterogenity (say in the parameters prescribing the firing rate function) and also allow for stochastic forcing. We now treat each of these in turn.

4.1. **Threshold fluctuation.** For a Heaviside firing rate function Brackley and Turner [13] have considered temporal correlations in a fluctuating threshold (taken to be a Gaussian random variable). Using a mixture of numerics and analysis they investigated how temporal correlations in the threshold affected the shape and speed of wave fronts. Here we pursue a similar analysis, focusing on a homogenous kernel with $w(x,y) = \phi(x-y)$, and analyse the effects of spatial correlations in the threshold. The firing threshold $h(x)$ is chosen to fluctuate around a mean value $\overline{h}$, such that $h(x) = \overline{h} + \delta h(x)$ where

$$\langle \delta h(x) \rangle_x = 0, \qquad \langle \delta h(x), \delta h(x+y) \rangle_x = a\mathrm{e}^{-|y|/\nu}/(2\nu). \tag{32}$$

Choosing large ν and small a gives a small slowly varying fluctuation in the firing threshold about a mean value $\overline{h}$. In the absence of any fluctuations ($a = 0$) the speed of the front is given by (13). Now, considering $\delta h \ll 1$, we expand (13) as

$$c = \frac{1-2\overline{h}}{2\overline{h}} + \frac{1}{2\overline{h}} \sum_{n=1}^{\infty} \left(-\frac{\delta h}{\overline{h}} \right)^n. \tag{33}$$

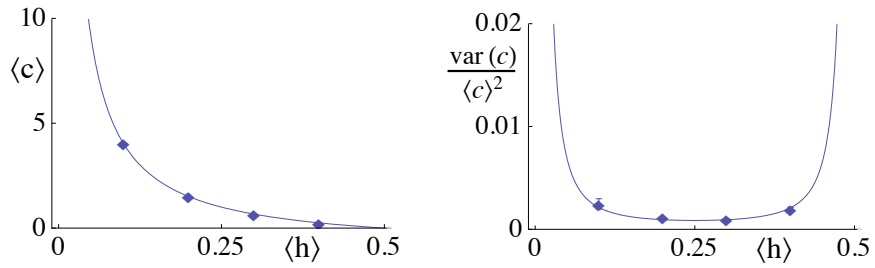

FIGURE 5. Mean (left) and scaled variance (right) of the wave front speed as a function of the threshold. $\langle \delta h(x)^2 \rangle_x = 1.35 \times 10^{-5}$.

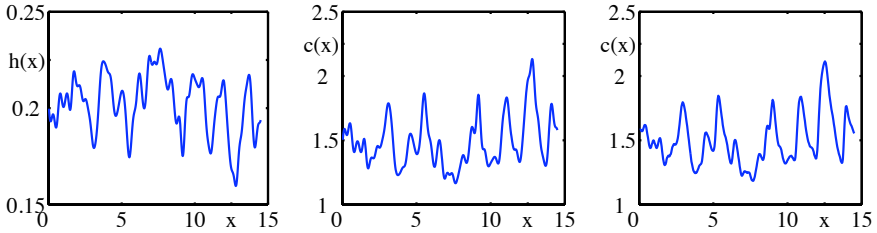

FIGURE 6. Left: Fluctuating firing threshold $h(x)$ for $\overline{h} = 0.2$, $a = 1$ and $\nu = 0.2$. Middle: $c(x) = (1 - 2h(x))/(2h(x))$. Right: Corresponding simulation results. (These were generated using a 4th order Runge-Kutta scheme with spatial-temporal discretisation $\Delta x = \Delta t = 0.025$ with a domain size $N \times \Delta x = 50$ and $N = 2000$. Fast Fourier transforms were used to calculate convolution terms).

From this we may calculate the average speed as

$$\langle c \rangle = \frac{1 - 2\overline{h}}{2\overline{h}} + \frac{1}{2\overline{h}} \sum_{n=1}^{\infty} (2n-1)!! \frac{\langle \delta h^2 \rangle^n}{\overline{h}^{2n}} \tag{34}$$

where !! denotes double factorial. The centered variance can also be found as

$$\langle (c - \langle c \rangle)^2 \rangle = \frac{1}{4\overline{h}^2} \left(\frac{\langle \delta h^2 \rangle}{\overline{h}^2} + 8 \frac{\langle \delta h^2 \rangle^2}{\overline{h}^4} + 69 \frac{\langle \delta h^2 \rangle^3}{\overline{h}^6} + \dots \right). \tag{35}$$

Plots of $\langle c \rangle$ and $\langle (c - \langle c \rangle)^2 \rangle / \langle c \rangle^2$ are shown in Fig. 5 using the formulas above as well as data from direct numerical simulations (where the wave speed is determined from simulation data simply by recording where a front crosses the mean firing threshold at every time step). We see that there is very good agreement between the small perturbation analysis and direct simulations of the model. This suggests that to a first approximation we may (for a given realisation of the threshold function) write

$$c(x) = \frac{1 - 2h(x)}{2h(x)}. \tag{36}$$

A plot of a realisation of $h(x)$ as well as the corresponding prediction from (36) and results from simulations are shown in Fig. 6, highlighting the usefulness of this simple ansatz for wave speed.

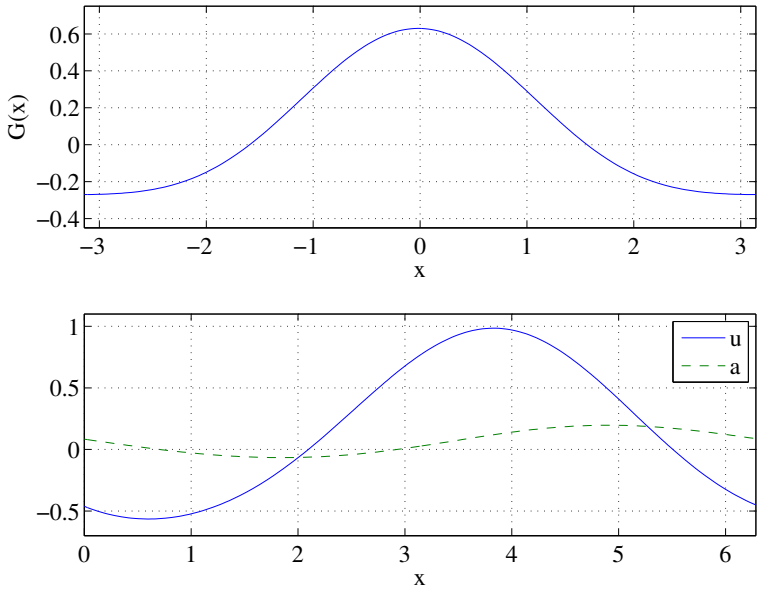

FIGURE 7. Top: $G(x)$ as given by (39). Bottom: a leftward moving *bump* of activity. Other parameters: $\beta = 20$, $h = 0.4$ and $B = 0.4$.

4.2. **Spatial parameter heterogeneity.** Here we pursue models with some form of adaptation [1] and show how to construct travelling waves in the presence of spatial parameter heterogeneity. For concreteness we consider a 1D system of the form

$$u_t(x,t) = -u(x,t) + \int_0^{2\pi} \mathrm{d}y G(x-y) f(u(y,t)) - a(x,t), \tag{37}$$

$$\tau a_t(x,t) = Bu(x,t) - a(x,t), \tag{38}$$

where

$$G(x) \equiv 0.09 + 0.45\cos x + 0.09\cos(2x), \tag{39}$$

and f is given by (2). As seen in Fig. 7 (top), $G(x)$ is of Mexican hat type, with local excitation and distal inhibition. The strength of the negative feedback is B and its timescale is τ, which we fix at $\tau = 15$. Note that the domain is now $[0, 2\pi]$, with periodic boundary conditions. Models of this form have been studied elsewhere [17, 18], and a typical, spatially-localised, moving *bump* of activity is shown in Fig. 7 (bottom).

In a coordinate frame moving with speed c, equations (37)-(38) are written

$$u_t(\xi,t) = cu_\xi(\xi,t) - u(\xi,t) + \int_0^{2\pi} \mathrm{d}y G(\xi-y) f(u(y,t)) - a(\xi,t), \tag{40}$$

$$a_t(\xi,t) = ca_\xi(\xi,t) + \frac{Bu(\xi,t) - a(\xi,t)}{\tau}. \tag{41}$$

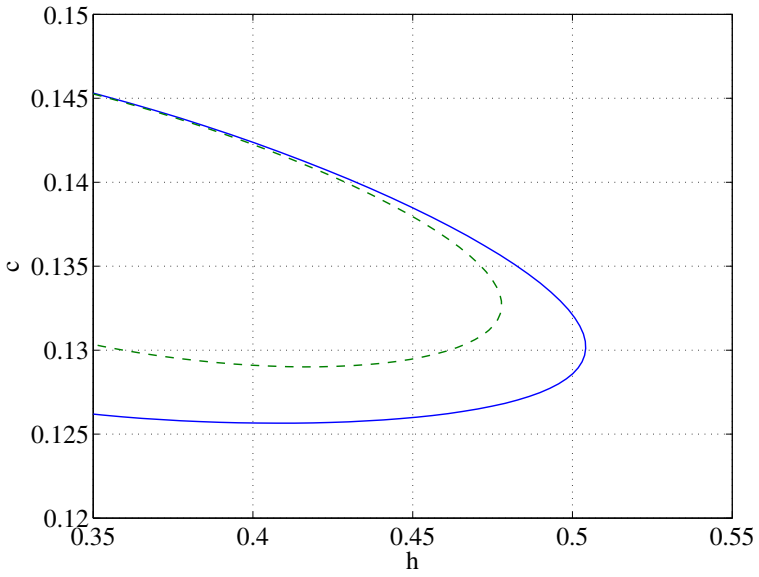

FIGURE 8. Speed of a bump of activity as a function of firing rate threshold h. Solid line: $\beta = 20$. Dashed line: β is spatial white noise (see text for details). Upper branches are stable, lower unstable. Other parameters: $\tau = 15$ and $B = 0.4$.

Bump solutions such as the one shown in Fig. 7 (bottom) are steady states of (40)-(41), i.e. satisfy

$$0 = cu_\xi(\xi) - u(\xi) + \int_0^{2\pi} dy G(\xi - y) f(u(y)) - a(\xi), \tag{42}$$

$$0 = ca_\xi(\xi) + \frac{Bu(\xi) - a(\xi)}{\tau}, \tag{43}$$

where c is equal to the speed of the bump. However, due to the translational invariance of solutions of (42)-(43), there is actually a continuum of such solutions related by translations in x. To remove this degeneracy, and in order to find c, we append the following *pinning* equation to (42)-(43):

$$\int_0^{2\pi} \frac{\partial \widehat{u}}{\partial x} (u - \widehat{u}) \ dx = 0, \tag{44}$$

where $\widehat{u}(x)$ is a *template* function [19], chosen to be $\cos(x)$ in this case. Equation (44) is the result of minimising the L^2 norm between u and $\widehat{u}$ [20, 21]. After suitably discretising eqns. (42)-(44) in space, solutions of the resulting system can be followed as parameters are varied, using (for example) pseudo-arclength continuation. An example of the results obtained is shown in Fig. 8 (solid line) where we plot c as a function of h for $\beta = 20$. We see that a stable and unstable bump are destroyed in a saddle-node bifurcation as h is increased.

The form of (42)-(44) suggests that one could introduce spatial heterogeneity to them, average over many realisations of this heterogeneity, and then solve the resulting equations in order to determine the effects of this heterogeneity. As an example, consider β (the gain of the firing rate function f) to be spatial white

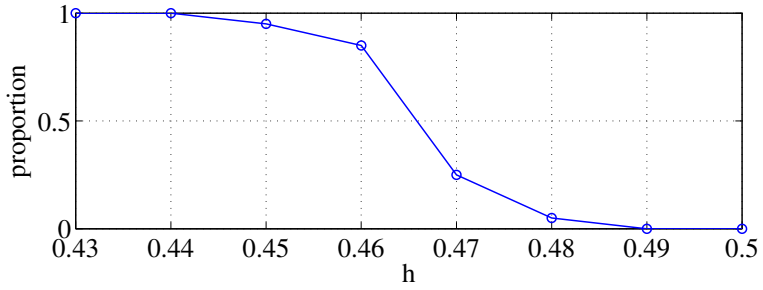

FIGURE 9. Proportion of simulations showing successful propagation of a bump as a function of h. Other parameters: $B = 0.4$.

noise. In practice, this means that at each of the 1000 spatial points used in the calculation of the term $\int_0^{2\pi} \mathrm{d}y G(\xi - y) f(u(y))$ in (42), β is chosen independently from a uniform distribution on $[m - \Delta, m + \Delta]$. Let $\beta^i(x)$ be the ith realisation of this process. We expect that solving the averaged system

$$0 = cu_\xi(\xi) - u(\xi) + \left\langle \int_0^{2\pi} \mathrm{d}y G(\xi - y) f[u(y), \beta^i(y)] \right\rangle_i - a(\xi), \tag{45}$$

$$0 = ca_\xi(\xi) + \frac{Bu(\xi) - a(\xi)}{\tau}, \tag{46}$$

$$0 = \int_0^{2\pi} \frac{\partial \widehat{u}}{\partial x} (u - \widehat{u}) \ \mathrm{d}x, \tag{47}$$

where the angled brackets indicate averaging over i and

$$f[u, \beta] = \frac{1}{1 + \mathrm{e}^{-\beta(u-h)}}, \tag{48}$$

will give information about the behaviour of (37)-(38) for a typical realisation of the $\beta^i(x)$. The results of solving (45)-(47) when $m = \Delta = 20$ are shown in Fig. 8 (dashed line). (We average over 2500 realisations of the $\beta^i(x)$. Increasing this number, or increasing the number of spatial points used to calculate the integral $\int_0^{2\pi} \mathrm{d}y G(\xi - y) f(u(y))$ does not qualitatively change the results presented.) From Fig. 8 we see that including such heterogeneity should (i) lower the maximum value of h for which a moving bump exists, and (ii) slightly decrease the speed of a stable moving bump. To illustrate that the first effect occurs we plot in Fig. 9, for several values of h, the proportion of 20 simulations for which a moving bump propagates, where (for fixed h) each of the 20 simulations uses a different realisation of $\beta(x)$. We see the gradual failure of propagation and, for example, that at $h = 0.49$ none of the simulations showed a propagating bump, whereas from Fig. 8, if β was constant over space, a stable bump would propagate at this parameter value. We also observed numerically that such spatial disorder does slightly decrease the stable bump's speed (not shown).

4.3. **Neural field models driven by temporal noise.** Another method for incorporating randomness in a neural field model is to drive it with spatio-temporal noise. For simplicity we focus here on purely temporal noise; we will use some of the ideas presented in [21].

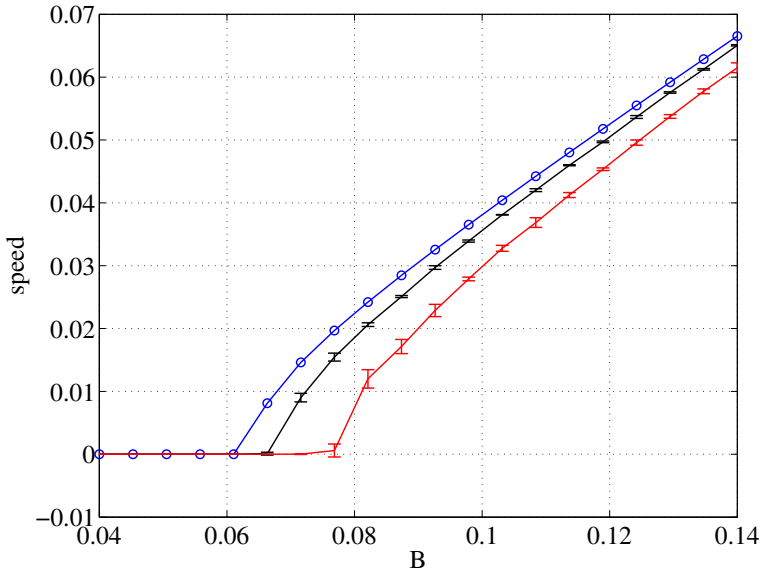

FIGURE 10. Speed of a moving bump solution of (51)-(52) for (from top to bottom) $D = 0$, 0.001 and 0.003. At each value of B, 5 simulations of duration 1000 time units were performed and the mean speed for each simulation was measured. The mean and standard deviation of these 5 speeds are plotted. Other parameters: $\tau = 5$, $h = 0.4$, $\beta = 20$ and $\gamma = 1$.

Consider the model

$$u_t(x,t) = -u(x,t) + \int_0^{2\pi} \mathrm{d}y G(x-y) f(u(y,t)) - a(x,t), \tag{49}$$

$$\tau a_t(x,t) = Bf(u(x,t)) - a(x,t), \tag{50}$$

which is very similar to (37)-(38), except that the dynamics of a are now nonlinear, as considered in, for example, [22]. Holding other parameters constant, if B (the strength of negative feedback) is decreased, the speed of a moving bump will decrease and reach zero at some non-zero value of B — see Fig. 10 (blue circles). (Put another way, a stable stationary bump goes unstable as B is increased through this value).

One question of interest is the effect of temporal noise on this bifurcation. To address this we replace (49) by $u_t \to u_t + \eta$ where $\eta(t)$ is coloured noise with $\langle \eta(t) \rangle = 0$ and $\langle \eta(t)\eta(s) \rangle = D\gamma \exp(-\gamma|t-s|)$. D is the noise intensity and $1/\gamma$ is the correlation time of the noise. Moving to a coordinate frame travelling at speed $c(t)$, (49)-(50) become

$$u_t(\xi,t) = c(t)u_\xi(\xi,t) - u(\xi,t) + \int_0^{2\pi} \mathrm{d}y G(\xi-y) f(u(y,t)) - a(\xi,t) + \eta(t), \tag{51}$$

$$a_t(\xi,t) = c(t)a_\xi(\xi,t) + \frac{Bf(u(\xi,t)) - a(\xi,t)}{\tau}. \tag{52}$$

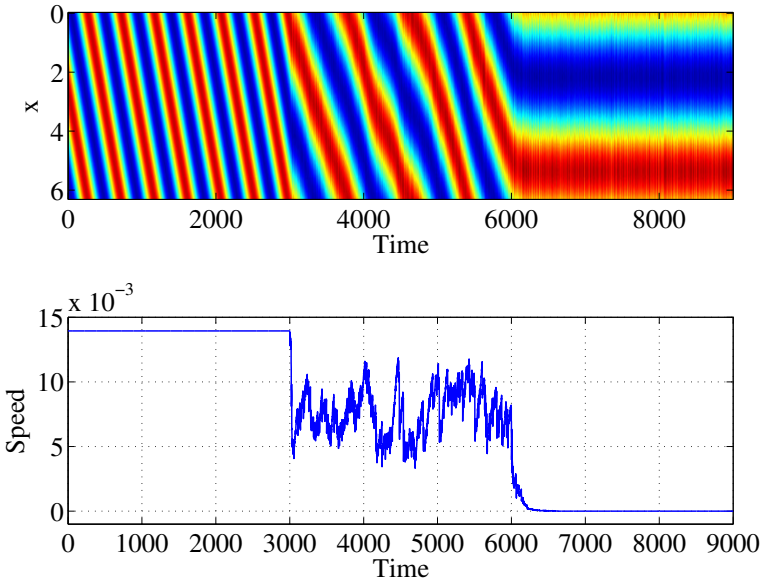

FIGURE 11. Top: simulation of (49)-(50) with additive noise and $B = 0.07$ for $D = 0$ $(0 < t < 3000)$, $D = 0.001$ $(3000 < t < 6000)$ and $D = 0.003$ $(t > 6000)$. $u(x,t)$ is shown colour-coded. Bottom: instantaneous bump speed extracted from the simulation in the top panel. Other parameters: $\tau = 5$, $h = 0.4$, $\beta = 20$ and $\gamma = 1$.

Although we can no longer find fixed points of (51)-(52) because of the presence of the noise term $\eta(t)$, we can still *freeze* solutions using (for example) (44) and simulate (51)-(52) with (44) for long periods of time, gathering statistics on $c(t)$, which is now a random variable. Some results are shown in Fig. 10 where we have used as a template a typical profile of u in the absence of noise. We see that increasing the amplitude of the noise decreases the bump's speed and moves the bifurcation to higher values of B. This is an example of noise *delaying* a bifurcation [23], and qualitatively similar results were found in [24, 25], where the authors considered spatially-discretised versions of models similar in form to (49)-(50) with additive noise. To demonstrate the results shown in Fig. 10, we show in Fig. 11 a simulation in which the noise intensity D is increased at two points in time, with all other parameters held constant. We see clearly the slowing down and then stopping of the bump. This can be regarded as a noise-induced bifurcation [26] which is easily understood by observing from Fig. 10 that for $D = 0$, $B = 0.07$ is to the right of the bifurcation (i.e. only moving bumps are stable) whereas for $D = 0.003$, $B = 0.07$ is to the left of the bifurcation, and the only stable state is a stationary bump.

5. **Discussion.** It is hard even at a first approximation to view the brain as a homogeneous system and so there is a pressing need to develop a set of mathematical tools for the study of waves in heterogeneous media that can be used in brain modelling. Homogenization is one natural multi-scale approach that can be utilised in this regard, and we have revisited the mathematical foundations of this approach in the context of non-local integral models that arise in neural field modelling. As a perturbation technique it requires that modulation on the micro-scale be both small

in amplitude and rapidly varying in space, and as such is limited in its range of applicability. For the special case of a Heaviside firing rate function we have shown how improved results can be obtained (circumventing the need for rapid spatial modulation) using an interface approach. One important observation, previously made by Bressloff [9], is that modulation of synaptic connectivity can lead to a slowing down of travelling waves and ultimately result in wave propagation failure. We have also considered other forms of natural disorder in this paper, including threshold fluctuations, parameter heterogeneity and stochastic forcing. Fluctuations of the firing threshold (spatial or temporal) can, in some scenarios, lead to an increase in wave speed, while additive noise can act rather differently and actually slow down or pin a wave. The mathematical toolbox for rigorously analysing these phenomenon does not yet exist and we have relied mainly on numerical simulations to gain insight. However, even here it has been interesting to consider how to define the notion of a travelling wave (in a system with broken translation invariance) and informative to adapt recent ideas developed for the numerical study of waves in stochastic PDEs [21]. In this sense it is likely that other ideas from applied dynamical systems [27] may be usefully adapted for the study of non-local random neural systems.

We have focused mainly on developing results in one spatial dimension and it remains to perform the extension to two spatial dimensions. Although both homogenization and interface formalisms go over naturally to two spatial dimensions the solution of the resulting models will no doubt remain a challenge — if nothing else but for the reason that solutions in 2D can come in a variety of rich forms such as spiral waves, labyrinthine structures and replicating and rotating collections of bumps [28, 16]. A generalisation of the freezing approach discussed in Secs. 4.2-4.3 has been applied to spiral waves in reaction-diffusion systems [20, 29] and it should be possible to apply them to waves in 2D neural field models. The development of a 2D interface dynamics for translation invariant kernels is currently under development and is likewise expected to form the basis for a perturbation theory for modulated connectivities. These and related ideas will be presented elsewhere.

Appendix A. Here we give an outline of the derivation of the homogenized version of (1) by means of two-scale convergence techniques. The detailed derivation of (4) will be presented in a complementary paper [30]. We write the original model in the form

$$\frac{\partial}{\partial t}u_\varepsilon(x,t) = -u_\varepsilon(x,t) + \int_{-\infty}^{\infty} w^*(x'-x, \frac{x'}{\varepsilon}) f(u_\varepsilon(x',t))\mathrm{d}x', \tag{53}$$

where $w^*(x,y) = \phi(|x|/\sigma(y))/\sigma(y)$. The relationship between w and w^* is given by $w(x,y) = w^*(x-y, y/\varepsilon)$. It turns out that this formulation of a neural field model is tractable when using two scale convergence techniques.

We view (53) as a one-parameter family of neural field models, parametrized by ε. The initial value problem of (53) is, according to Potthast *et al.* [31], globally well-posed in the Banach space of bounded, continuous functions for connectivity functions which are uniformly bounded in both the supremum norm and the L^1-norm and satisfy a Hölder condition, and firing rate functions which take values between 0 and 1. One notable property is that the ε-dependent solution is uniformly bounded, where the bound depends on the supremum norm of the initial condition and the bounding constant of the connectivity function in the L^1-norm.

We assume from now on that the conditions prescribed in Potthast *et al.* [31] are fulfilled.

For our purposes we will need the existence and boundedness of solution u_ε in $L^2(\mathbb{R})$. From Theorem 3.2.1 in Faye *et al.* [32], which is a straightforward adaptation of a classical result by Hale *et al.* [33] for first order functional differential equations, we get the following result:

Lemma 1. *Assume that $w^* \in L^2(\mathbb{R})$ and that the initial condition $u_\varepsilon(x,0) = U(x)$ is square integrable, i.e. $U \in L^2(\mathbb{R})$. Then there is a unique solution $u_\varepsilon \in L^2([0,T];L^2(\mathbb{R}))$ of (53) which obeys the uniform bounds*

$$\|u_\varepsilon\|_{L^\infty([0,T];L^2(\mathbb{R}))} \leq C_1 \left(\|U\|_{L^2(\mathbb{R})} + \|w^*\|_{L^2(\mathbb{R})}\right), \tag{54}$$

and

$$\|u_\varepsilon\|_{L^2([0,T];L^2(\mathbb{R}))} \leq C_1 \left(\|U\|_{L^2(\mathbb{R})} + \|w^*\|_{L^2(\mathbb{R})}\right). \tag{55}$$

for some constants $C_1 > 0$ and $T > 0$.

Just as in [34, 35] we get the following results:

Lemma 2. *Let the initial condition $u_\varepsilon(x,0) = U(x)$ of (53) belong to the intersection $L^1(\mathbb{R}) \cap L^\infty(\mathbb{R})$ and assume that*

$$\sup_{x\in\mathbb{R}} \{ \int_{-\infty}^{\infty} w^*(x,y)\mathrm{d}y \} \leq C$$

for some positive constant $C > 0$. Then there exists a unique $u_\varepsilon \in C(\mathbb{R}_0^+; L^1(\mathbb{R}) \cap L^\infty(\mathbb{R}))$ satisfying (53). Moreover, we have the uniform bounds

$$\max_{0\leq t\leq T} \|u_\varepsilon\|_{L^1(\mathbb{R})} \leq C\|U\|_{L^1(\mathbb{R})}$$

and

$$\max_{0\leq t\leq T} \|u_\varepsilon\|_{L^\infty(\mathbb{R})} \leq C\|U\|_{L^\infty(\mathbb{R})}$$

for some $T > 0$.

The proofs of Lemma 1 and Lemma 2 will be presented in a forthcoming paper [30].

Next, let us define the concept of two-scale convergence: Let $\mathbb{T}$ denote the 1-dimensional unit torus (or unit circle) and let $Y = [0,1]$. We identify the Y-periodic functions by those functions that are defined on $\mathbb{T}$ and introduce functions $\rho \in L^2(\mathbb{R} \times \mathbb{T})$ and consider their traces $\rho(x, x/\varepsilon)$. Assume that $\{v_\varepsilon\}$ is a bounded sequence in $L^2(\mathbb{R})$. The sequence $\{v_\varepsilon\}$ is said to *two-scale converge* to $v \in L^2(\mathbb{R}; L^2(\mathbb{T}))$ if

$$\int_{-\infty}^{\infty} v_\varepsilon(x)\rho(x, \frac{x}{\varepsilon})\mathrm{d}x \to \int_{-\infty}^{\infty}\int_Y v(x,y)\rho(x,y)\mathrm{d}y\mathrm{d}x. \tag{56}$$

as $\varepsilon \to 0$ for all test functions ρ. A crucial step consists of constructing an admissible class X of test functions ρ so that for any bounded sequence $\{v_\varepsilon\} \in L^2(\mathbb{R})$ we have the convergence (56). It turns out that we obtain two-scale convergence if X is identified with the space $L^2(\mathbb{R}; C(\mathbb{T}))$.

$L^2(\mathbb{R}; L^2(\mathbb{T}))$ denotes the space of those functions which are square integrable both in the x and in the y-variable and are Y-periodic in y. The space $L^2(\mathbb{R}; C(\mathbb{T}))$ is

the space of functions which are square integrable in the x variable and continuous in the y variable and Y-periodic in the y variable.

The convergence in (56) is nothing but a weak convergence in L^2-spaces where the key ingredient is that the test functions ρ vary on two scales, i.e. on the global scale x and on the local microscale y. By parameterizing (in ε) and substituting $y = x/\varepsilon$ the limit process will then capture a two-scales limit $v = v(x, y)$ having the same period as the two-scales test function ρ. From a heuristic point of view, the two-scales limit function $v = v(x, y)$ is the first term in a two-scales asymptotic expansion of v_ε. This means that the two-scale convergence rigorously justifies the existence of $v = v(x, y)$. If we have more regularity so that the sequence $\{v_\varepsilon\}$ is bounded in $H^1(\mathbb{R})$, then two-scale convergence yields the existence of the first two terms in a two-scales asymptotic expansion of v_ε. In that case one can rigorously justify that $v_\varepsilon(x) \sim v(x) + \varepsilon v_1(x, x/\varepsilon)$.

Now, according to Remark 7 in [36] it is possible to modify the definition of two-scale convergence in L^2-spaces to obtain a definition of two-scale convergence in L^1-spaces; see also [37]. The test functions are chosen here to be continuous with compact support in x and continuous and Y-periodic in y. It is crucial that we can include the L^1-case since it turns out in the application of two-scale convergence to the convolution integral in (1) that one of the terms is assumed to two-scale converge in L^1. So the fundamental question now is how to determine the limit of the convolution term as $\varepsilon \to 0$. The following theorem which originally was proved by Visintin [37] gives the answer to that question:

Theorem 1. *Suppose that $\{v_\varepsilon\}$ is a sequence of two-scale functions converging to $v \in L^2(\mathbb{R}; L^2(\mathbb{T}))$ and that $\{w_\varepsilon\}$ is two-scale converging to $w \in L^1(\mathbb{R}; L^1(\mathbb{T}))$. Then the convolution integral*

$$[w_\varepsilon \otimes v_\varepsilon](x) \equiv \int_{-\infty}^{\infty} w_\varepsilon(x' - x) v_\varepsilon(x') \mathrm{d}x', \tag{57}$$

two-scale converges to the double-convolution integral

$$[w^* \otimes\otimes\, v](x, y) \equiv \int_{-\infty}^{\infty} \int_Y w^*(x' - x, y' - y) v(x', y') \mathrm{d}y' \mathrm{d}x', \tag{58}$$

as $\varepsilon \to 0$ in $L^2(\mathbb{R}; L^2(\mathbb{T}))$. The limit (58) (which is Y-periodic in the variable y), is called the spatial two-scale convolution limit.

Now, the sequence of connectivity kernels $\{w_\varepsilon\}$ defined by $w_\varepsilon(z) = w^*(z, x'/\varepsilon)$ where w^* is given by (5), is by assumption a bounded sequence in $L^1(\mathbb{R})$. We then have the two-scale convergence $w^*(z, x'/\varepsilon) \to w^*(z, y)$ in $L^1(\mathbb{R}; L^1(\mathbb{T}))$. Since u_ε by Lemma 1 is bounded in $L^2(\mathbb{R})$, u_ε will two-scale converge to some function $u \in L^2(\mathbb{R}; L^2(\mathbb{T}))$, $u = u(x, y)$. As f is a bounded and monotone function with values between 0 and 1, the sequence $v_\varepsilon = f \circ u_\varepsilon$ two-scale converges to $v = f \circ u \in L^2(\mathbb{R}; L^2(\mathbb{T}^1))$. (See Theorem 3.1 in [38] for a recent proof.) Notice that we by Lemma 2 can also conclude that $v_\varepsilon = f \circ u_\varepsilon$ two-scale converges to $v = f \circ u \in L^1(\mathbb{R}; L^1(\mathbb{T}^1))$. From Visintin's theorem (Theorem 1), we conclude that the one-parameter family of neural field models (53) approaches in the two-scale sense as $\varepsilon \to 0$ the nonlocal evolution equation given by (4). One can prove, by using the same techniques as in Potthast *et al.* [31] that the initial value problem of (4) is globally well-posed. Finally it is worth pointing out that the multiscale convergence

techniques are applicable to neural field models in several space dimensions and also with heterogeneity in parameters of the firing rate function.

REFERENCES

[1] S Coombes, *Waves, bumps, and patterns in neural field theories*, Biological Cybernetics, **93** (2005), 91–108.

[2] H. R. Wilson and J. D. Cowan, *Excitatory and inhibitory interactions in localized populations of model neurons*, Biophysical Journal, **12** (1972), 1–24.

[3] H. R. Wilson and J. D. Cowan, *A mathematical theory of the functional dynamics of cortical and thalamic nervous tissue*, Kybernetik, **13** (1973), 55–80.

[4] S. Amari, *Homogeneous nets of neuron-like elements*, Biological Cybernetics, **17** (1975), 211–220.

[5] S. Amari, *Dynamics of pattern formation in lateral-inhibition type neural fields*, Biological Cybernetics, **27** (1977), 77–87.

[6] G. B. Ermentrout and D. Kleinfeld, *Traveling electrical waves in cortex: Insights from phase dynamics and speculation on a computational role*, Neuron, **29** (2001), 33–44.

[7] B. W. Connors and Y. Amitai, *Generation of epileptiform discharges by local circuits in neocortex*, in "Epilepsy: Models, Mechanisms and Concepts" (ed. P A Schwartzkroin), Cambridge University Press, (1993), 388–424.

[8] O. Faugeras, F. Grimbert and J.-J. Slotine, *Absolute stability and complete synchronization in a class of neural fields models*, SIAM Journal on Applied Mathematics, **69** (2008), 205–250.

[9] P. C. Bressloff, *Traveling fronts and wave propagation failure in an inhomogeneous neural network*, Physica D, **155** (2001), 83–100.

[10] H. Schmidt, A. Hutt and L. Schimansky-Geier, *Wave fronts in inhomogeneous neural field models*, Physica D, **238** (2009), 1101–1112.

[11] S. Coombes and C. R. Laing, *Pulsating fronts in periodically modulated neural field models*, Physical Review E, **83** (2011), 011912.

[12] C. A. Brackley and M. S. Turner, *Persistent fluctuations of activity in undriven continuum neural field modles with power-law connections*, Physical Review E, **79** (2009), 011918.

[13] C. A. Brackley and M. S. Turner, *Random fluctuations of the firing rate function in a continuum neural field model*, Physical Review E, **75** (2007), 041913.

[14] J. Keener, *Homogenization and propagation in the bistable equation*, Physica D, **136** (2000), 1–17.

[15] G. Nguetseng, *A general convergence result of a functional related to the theory of homogenization*, SIAM Journal on Mathematical Analysis, **20** (1989), 608–623.

[16] M. R. Owen, C. R. Laing and S. Coombes, *Bumps and rings in a two-dimensional neural field: Splitting and rotational instabilities*, New Journal of Physics, **9** (2007), 378.

[17] P. C. Bressloff and S. E. Folias, *Front bifurcations in an excitatory neural network*, SIAM Journal on Applied Mathematics, **65** (2004), 131–151.

[18] D. J. Pinto and G. B. Ermentrout, *Spatially structured activity in synaptically coupled neuronal networks. I. Traveling fronts and pulses*, SIAM Journal on Applied Mathematics, **62** (2001), 206–225.

[19] C. W. Rowley, I. G. Kevrekidis, J. E. Marsden and K. Lust, *Reduction and reconstruction for self-similar dynamical systems*, Nonlinearity, **16** (2003), 1257–1275.

[20] W.-J. Beyn and V. Thümmler, *Freezing solutions of equivariant evolution equations*, SIAM Journal on Applied Dynamical Systems, **3** (2004), 85–116.

[21] G. J. Lord and V. Thümmler, *Freezing stochastic travelling waves*, arXiv:1006.0428, 2010.

[22] S. Coombes and M. R. Owen, *Evans functions for integral neural field equations with Heaviside firing rate function*, SIAM Journal on Applied Dynamical Systems, **34** (2004), 574–600.

[23] L. Fronzoni, R. Mannella, P. V. E. McClintock and F. Moss, *Postponement of Hopf bifurcations by multiplicative colored noise*, Physical Review A, **36** (1987), 834.

[24] C. R. Laing and A. Longtin, *Noise-induced stabilization of bumps in systems with long-range spatial coupling*, Physica D, **160** (2001), 149–172.

[25] C. R. Laing, T. A. Frewen and I. G. Kevrekidis, *Coarse-grained dynamics of an activity bump in a neural field model*, Nonlinearity, **20** (2007), 2127–2146.

[26] B. Ermentrout and D. Saunders, *Phase resetting and coupling of noisy neural oscillators*, Journal of Computational Neuroscience, **20** (2006), 179–190.

[27] J. Xin, "An Introduction to Fronts in Random Media," Surveys and Tutorials in the Applied Mathematical Sciences, **5**, Springer, New York, 2009.
[28] C. R. Laing, *Spiral waves in nonlocal equations*, SIAM Journal on Applied Dynamical Systems, **4** (2005), 588–606.
[29] S. Hermann and G. A. Gottwald, *The large core limit of spiral waves in excitable media: A numerical approach*, SIAM Journal on Applied Dynamical Systems, **9** (2010), 536–567.
[30] N. Svanstedt and J. Wyller, *A one population Wilson-Cowan model with periodic microstructure*, in preparation, 2011.
[31] R. Potthast and P. B. Graben, *Existence and properties of solutions for neural field equations*, Mathematical Methods in the Applied Sciences, **33** (2010), 935–949.
[32] G. Faye and O. Faugeras, *Some theoretical and numerical results for delayed neural field equations*, Physica D, **239** (2010), 561–578.
[33] J. K. Hale and S. M. V. Lunel, "Introduction to Functional-Differential Equations," Applied Mathematical Sciences, **99**, Springer-Verlag, New York, 1993.
[34] L. I. Ignat and J. D. Rossi, *Decay estimates for nonlocal problems via energy estimates*, Journal de Mathématiques Pures et Appliquées, **92** (2009), 163–187.
[35] A. F. Pazoto and J. D. Rossi, *Asymptotic behaviour for a semilinear nonlocal equation*, Asymptotic Analysis, **52** (2007), 143–155.
[36] A. Holmbom, J. Silfver, N. Svanstedt and N. Wellander, *On two-scale convergence and related sequential compactness topics*, Applications of Mathematics, **51** (2006), 247–262.
[37] A. Visintin, *Towards a two-scale calculus*, ESAIM: Control, Optimisation and Calculus of Variations, **12** (2006), 371–397.
[38] A. Visintin, *Two-scale convergence of some integral functionals*, Calculus of Variations and Partial Differential Equations, **29** (2007), 239–265.

Received April 2011; revised July 2011.

E-mail address: stephen.coombes@nottingham.ac.uk
E-mail address: c.r.laing@massey.ac.nz
E-mail address: pmxhs@exmail.nottingham.ac.uk
E-mail address: nilss@chalmers.se
E-mail address: john.wyller@umb.no